Author Manuscript

Author Manuscript

Author Manuscript

Author Manuscript

HHS Public Access

Author manuscript

J Nucl Cardiol. Author manuscript; available in PMC 2021 February 02.

Published in final edited form as:

J Nucl Cardiol. 2019 December ; 26(6): 1946–1957. doi:10.1007/s12350-018-1287-7.

Simultaneous determination of dynamic cardiac metabolism and function using PET/MRI

Gregory P. Barton, PhD[1,6], **Lauren Vildberg**[1,6], **Kara Goss, MD**[1,3,6], **Niti Aggarwal, MD**[2,4], **Marlowe Eldridge, MD**[1,5,6], **Alan B. McMillan, PhD**[4]

[1]Department of Pediatrics, University of Wisconsin-Madison,

[2]Division of Cardiovascular Disease Department of Medicine, University of Wisconsin-Madison,

[3]Department of Medicine, University of Wisconsin-Madison,

[4]Department of Radiology, University of Wisconsin-Madison,

[5]Department of Biomedical Engineering, University of Wisconsin-Madison,

[6]Rankin Laboratory of Pulmonary Medicine, University of Wisconsin-Madison

Abstract

Background—Cardiac metabolic changes in heart disease precede overt contractile dysfunction. However, metabolism and function are not typically assessed together in clinical practice. The purpose of this study was to develop a cardiac positron emission tomography/magnetic resonance (PET/MR) stress test to assess the dynamic relationship between contractile function and metabolism in a preclinical model.

Methods—Following an overnight fast, healthy pigs (45–50kg) were anesthetized and mechanically ventilated. ^{18}F-fluorodeoxyglucose (^{18}F-FDG) solution was administered intravenously at a constant rate of 0.01ml/s for 60 minutes. A cardiac PET/MR stress test was performed using normoxic gas (F_IO_2 = 0.209) and hypoxic gas (F_IO_2 = 0.12). Simultaneous cardiac imaging was performed on an integrated 3T PET/MR scanner.

Results—Hypoxic stress induced a significant increase in heart rate, cardiac output, left ventricular (LV) ejection fraction (EF), and peak torsion. There was a significant decline in arterial SpO_2, LV end-diastolic and end-systolic volumes in hypoxia. Increased LV systolic function was coupled with an increase in myocardial FDG uptake (Ki) during hypoxic stress.

Conclusion—PET/MR with continuous FDG infusion captures dynamic changes in both cardiac metabolism and contractile function. This technique warrants evaluation in human cardiac disease for assessment of subtle functional and metabolic abnormalities.

Introduction

Heart disease is frequently preceded by metabolic remodeling of the myocardium characterized by a switch from fatty acid metabolism to increased reliance on glucose

Corresponding author: Gregory P. Barton, PhD, Post-Doctoral Fellow, UW School of Medicine and Public Health, Department of Pediatrics, 600 Highland Ave. H6/551 CSC, Madison, WI 53792, (608) 265-5095, gpbarton@pediatrics.wisc.edu.

Author Manuscript Author Manuscript Author Manuscript Author Manuscript

utilization (1–9). In early stages of heart failure, systolic function may be preserved despite fundamental metabolic changes. Indeed, in the setting of systemic and pulmonary hypertension there is an association between increased left ventricular (LV) and right ventricular (RV) glucose metabolism and reduced LV and RV contractile function, respectively (9, 10). Hence, the glucose analog ^{18}F-fluorodexyglucose (^{18}F-FDG) offers an opportunity for assessment of glucose metabolism using positron emission tomography (PET) in the setting of heart disease. ^{18}F-FDG is an advantageous radiotracer as it is 1) considered an irreversible substrate, since it is trapped in the early metabolic pathway (after phosphorylation) and 2) ^{18}F-FDG is a universal and low-cost agent for studies in cardiac metabolism.

Currently, cardiac imaging studies use a bolus injection of ^{18}F-FDG in order to determine glucose utilization (3, 10, 11). With a bolus application, the uptake of the radiotracer is relatively stable after 30 minutes, enabling basic methods such as standard uptake values (SUV) to be used in assessment of baseline glucose metabolism. This currently used method has several potential confounds. First, glucose metabolism may not be at equilibrium over the course of a full experiment. Second, sequential measurements often made days or weeks apart introduce uncontrolled variables (12). Additionally, there may be substantial intrasubject variability between repeated scans, as recently identified by differentiation of task or stress dependent changes from baseline glucose metabolism in the brain using two separate PET scans (13, 14). Recently, a novel technique utilizing a continuous infusion of ^{18}F-FDG has been proposed to study cerebral glucose metabolism (12, 15). This technique uses a constant supply of ^{18}F-FDG during the entire scan, which enables the dynamic assessment of task-specific changes in glucose metabolism, and a similar methodology is applied herein.

In most clinical scenarios, cardiac metabolism and function are not assessed simultaneously. While existing clinical imaging modalities provide exquisite measures of cardiac function, most cardiac disease states cannot be fully captured by measuring function alone. Furthermore, previous studies performed in human subjects have performed no simultaneous acquisition of measures of cardiac metabolism and contractile function, and cardiac parameters are measured under resting conditions (3, 10). The induction of a physiological stressor, such as hypoxia or exercise, may elicit subclinical changes in cardiac function which are not typically observed under resting imaging conditions (16, 17). Finally, to determine their relationship, cardiac metabolism and contractile function must be imaged together, which requires the use of simultaneous PET and MR imaging. Therefore, the purpose of this study was to develop a novel methodology using cardiac PET/MR imaging to study the dynamic relationship between contractile function and metabolism using a rest-stress scenario in a preclinical model.

Methods

Animal preparation and Study design.

Domestic pigs 45–50 kg (n = 10, female = 5) were obtained from the Swine Research Training Center (SRTC) at UW-Madison. Following an overnight fast, the animals were anesthetized using telazol (5 mg/kg)/xylazine (1 mg/kg IM). An endotracheal tube was

Author Manuscript Author Manuscript Author Manuscript Author Manuscript

inserted and a mechanical ventilator connected to 21% O_2, and maintenance anesthetization was maintained with 2% isoflurane for the PET/MR imaging study. ^{18}F-FDG in saline solution was administered intravenously at a constant rate of 0.01 ml/s for 60 minutes for an injected dose of ~ 3.48 MBq/kg/hr using a syringe pump (Medrad Spectra Solaris, Bayer Healthcare LLC, Whippany, NJ) with initial activity = ~5 mCi, as performed previously in cerebral imaging (12). For assessment of plasma glucose and lactate, arterial blood samples were collected prior to the PET scan and approximately every 10 minutes (in between MR imaging sequences) after the start of ^{18}F-FDG infusion from a 7 French catheter inserted into the carotid artery. After 25–30 minutes of normoxic breathing (F_IO_2 = 0.209), hypoxic stress was induced by administering hypoxic air (F_IO_2 = 0.12). After approximately 10 minutes of settling time to equilibrate to a steady state hypoxic response, 25–30 minutes of continued imaging was performed as shown in Figure 1. Throughout the imaging protocol arterial oxygen saturation was assessed with pulse oximetry and blood pressure was monitored every two minutes with a sphygmomanometer. At the end of the imaging study, animals were euthanized by intravenous injection of Euthasol® (0.22 ml/kg sodium pentobarbital + sodium phenytoin). Animal housing and handling was carried out under the guidelines of the Institutional Animal Care and Use Committees and conducted in pathogen-free facilities that are accredited by the American Association of Accreditation of Laboratory Animal Care.

Simultaneous cardiac PET/MR imaging.

Dynamic, simultaneous cardiac PET/MR imaging was performed on an integrated 3T scanner (Signa PET/MR, GE Healthcare, Waukesha, WI). MRI measures consisted of cardiac-gated tagged and untagged short axis cine MR during breath holds with the following parameters: 35 cm FOV, 1.3 ms TE, 3.6 ms TR, matrix 224×224, slice thickness 7cm, covering the entire LV. PET data was acquired simultaneously with MRI. Reconstruction parameters for dynamic PET are as follows: 60 second frame duration, 45 cm FOV, matrix 192×192, 28 subsets, 2 iterations, VPFX-S, time-of-flight, and 5 mm smoothing. Short-axis cine MR images were analyzed in software Segment version 2.0 (http://segment.heiberg.se) to determine LV and RV volumes. Dynamic PET data was analyzed in custom MATLAB (The Mathworks, Natick, MA) software. Three dimensional regions of interest (ROIs) were manually drawn over the left ventricle plus septum (myocardial), in the triceps muscle (skeletal muscle), and blood pool (BP) utilizing the PET imaging comprising the temporal average of all dynamic activity. Example ROIs are shown in Figure 5. The ROIs were eroded by two cycles in order to control for partial volume effects. The average value from each ROI was extracted for each time point to extract time activity curves. The time activity curves of the myocardial and skeletal muscle ROIs were normalized by the time activity curve of the blood pool, to assess relative FDG uptake in active (myocardial) and passive (skeletal) muscle ROIs, which yields a near linear time activity ratio function. The slope of the time activity ratio (myocardium:BP and skeletal muscle:BP) was calculated for the normoxic and hypoxic time periods separately. Patlak analysis (15, 18) to measure the net uptake rate (K_i) of ^{18}F-FDG was performed using a home-built script written in MATLAB (The Mathworks Inc., Natick, MA) utilizing non-linear least squares fitting (lsqcurvefit). Myocardial glucose utilization rate was not calculated due to the known variability in the lumped constant during different metabolic

Author Manuscript Author Manuscript Author Manuscript Author Manuscript

states (19), which we believe would directly conflict with the rest-stress scenario used herein.

LV strain analysis.

Three slices from the LV (apex, mid and base) tagged short-axis cine MR images were used to analyze circumferential and radial dimensions (mean peak strain, systolic and diastolic strain rate, peak rotation and peak torsion) using Segment strain analysis module (http://segment.heiberg.se). Peak rotation is quantified by mean angular distance by all of the tracking points around an axis of rotation, which is centered on mid LV septum. Peak rotation is then defined by the difference in mean angular rotation in degrees between the apex and base. Peak torsion is calculated from the rotational difference of the heart for the most basal and apical slice chosen. The rotational difference is then normalized with the mean radius divided by the distance in the long-axis.

Statistical Analysis.

A paired t-test was used to determine differences between normoxia and hypoxia exposure for cardiovascular hemodynamics. Wilcoxon matched pairs signed rank test was used to determine differences in myocardial strain and kinetic PET assessments between normoxia and hypoxia. A linear regression was used to determine the relationship between LV EF and LV peak torsion. Repeated measures one-way ANOVA was used to determine differences in arterial plasma glucose and lactate changes over time (GraphPad Prism 6;GraphPad Software Inc., San Diego, CA). A P-value < 0.05 was considered significant.

Results

Hemodynamic changes from normoxia to hypoxia.

Transition from normoxia to hypoxia was associated with a decrease in arterial saturation from 99% to 71%. In response, there was an increase in heart rate (HR) (97 ± 3 beats/min vs 112 ± 4 beats/min), which in turn resulted in an increased cardiac output (CO) (3228 ± 145 ml/min vs 3931 ± 288 ml/min), LV ejection fraction (EF) (56 ± 1 vs 66 ± 2), and rate pressure product (RPP) (10767 ± 740 mmHg*beats/min vs 12759 ± 1138 mmHg*beats/min), respectively (Table I; $p<0.05$ for all). There was no change in LV stroke volume. In addition, end-diastolic volume (EDV) (61 ± 3 ml vs 54 ± 3 ml) and end-systolic volume (ESV) (27 ± 2 ml vs 18 ± 2 ml) decreased from normoxia to hypoxia, respectively (Figure 2) (Table I).

LV strain in response to hypoxia.

There were no differences in LV circumferential or radial strain (mean peak, systolic or diastolic strain rate) between normoxia and hypoxia. However, there was a significant difference in peak rotation and peak torsion in the LV during hypoxia as compared to normoxia ($p < 0.05$) (Table II). Figure 3 is a representative image of the tracking points and the axis of rotation that was used to determine LV strain with a representation of the circumferential and radial strain curves from the strain analysis. Additionally, we determined that peak torsion is significantly associated with LV EF (Figure 4).

Author Manuscript Author Manuscript Author Manuscript Author Manuscript

Changes in glucose metabolism.

The respective ROIs drawn to determine the time activity curves for skeletal muscle, myocardium, and blood pool are shown in Figure 5A. Representative Patlak plots for the myocardium and skeletal muscle (Figure 5B), and the slopes of the time activity curve (TAC) were determined in normoxia and hypoxia (Figure 5C). Myocardial net uptake rate (Ki) increased during hypoxia, whereas, glucose uptake rate decreased in resting skeletal muscle during hypoxia ($p < 0.05$) (Table III/Figure 6). The TAC ratio slope curve, defined as the ratio of the myocardial to BP slope of the PET data increased two-fold ($p < 0.05$), suggesting increased LV glucose utilization as a result of hypoxic stress as shown in Table III/Figure 6. Additionally, there was a significant decline in the skeletal muscle to BP slope in hypoxia (Table III/Figure 6).

Arterial plasma glucose and lactate changes.

There was a significant increase in arterial plasma lactate values during hypoxia as compared to normoxia ($p < 0.05$). There were no differences in arterial plasma glucose throughout the study duration (Figure 7), which supports the use of an image-derived input function for the Patlak modeling.

Discussion

The purpose of this study was to establish the feasibility of performing a serial rest-stress scenario using PET/MR to simultaneously image cardiac glucose metabolism (as measured by ^{18}F-FDG) and cardiac function in response to increased myocardial workload, using hypoxic gas ($F_IO_2 = 0.12$) as a physiological stressor. We focused on changes in left ventricular function in hypoxia due to previous work demonstrating increased myocardial workload (i.e. increased heart rate and systolic function) in the LV during hypoxia (20). When going from normoxia to hypoxia, there was a reduction in preload (LVEDV) combined with no change in afterload (MAP), suggestive of increased LV contractility. This was manifested as a 19% increase in LV EF coupled with a significant increase in ^{18}F-FDG uptake by the LV using both quantitative (K_i) and non-quantitative (myocardial/bloodpool slope ratio) analysis during continuous ^{18}F-FDG infusion. Additionally, we saw a significant reduction in the slope of the blood pool TAC during hypoxia, which suggests a systemic increase in glucose utilization, an expected response to hypoxia. The rise in arterial lactate concentration during hypoxia demonstrates a global increase in anaerobic glucose metabolism. These results demonstrate the capability of using simultaneous cardiac PET/MR to measure meaningful changes in cardiac function and metabolism with a rest-stress scenario within the same scanning protocol, which may have many potential applications clinically.

We chose to use acute hypoxia as a stressor in this proof-of-concept study utilizing this serial rest-stress technique combined with continuous infusion because of the well-known cardiac hemodynamic effects (16, 20–23) and augmentation of myocardial glucose uptake (24) induced by acute hypoxia. Acute hypoxia increases heart rate, cardiac output, and LV systolic function, all of which increase myocardial workload (16, 20–23), which corroborates our findings.

Author Manuscript Author Manuscript Author Manuscript Author Manuscript

Cardiac magnetic resonance tissue tagging permits intramyocardial displacement and strain to be measured noninvasively by examining the motion of identifiable points distributed throughout the myocardium (25–27). We found that LV EF increased in response to hypoxia, however, circumferential or radial strain parameters remained unchanged. Notably, we saw a significant increase in peak rotation and torsion in the LV in response to hypoxic stress compared to normoxic resting conditions. Myocardial torsion is a fundamental component of LV function (28). Torsion is produced due to the double helical nature of myocardial fibers, which results in systolic rotation in opposite directions between the apex and base of the left ventricle in the longitudinal axis (29–31). Although we did not observe an increase in LV strain in the circumferential or radial axis, LV torsion has been determined to be correlated with LV longitudinal strain (32). The increased LV EF in hypoxic conditions is significantly associated with an increase in LV peak torsion and possibly an increase in long-axis strain, although we did not perform long-axis strain analysis.

Previous works in ex vivo models using increased afterload or catecholamines to increase myocardial workload have demonstrated increased glucose utilization (33, 34). Increases in LV contractility, HR, CO, and rate pressure product (RPP) with acute hypoxia in our study demonstrate an increased myocardial workload which was coupled to a significant augmentation of glucose uptake into the LV during hypoxia. This finding of increased glucose utilization in the heart in our study is similar to the findings in the human heart, although the previous study did not measure cardiac contractile function (24). These findings are supported by a concomitant rise in arterial lactate during hypoxia, which suggests a global increase in anaerobic glycolysis. Further support of a systemic increase in glucose utilization was the finding of an approximate 4-fold reduction in the slope of the blood pool TAC. We used resting skeletal muscle as a reference tissue and found that FDG uptake was reduced in hypoxia, whereas, the myocardial FDG uptake was augmented in combination with increased myocardial work. Indeed, hypoxia and/or anoxia increases plasma membrane glucose transporters in cardiac muscle (35) which is an important adaptation to hypoxia due to restricted use of fatty acids at low oxygen levels (36, 37).

We utilized a novel approach to dynamically measure glucose utilization in the heart by administering ^{18}F-FDG via a continuous infusion. One group has used the continuous infusion approach to measure dynamic changes in glucose uptake in the brain (12). These investigators combined continuous infusion of ^{18}F-FDG with fMRI (PET/MR) at rest and used visual stimulation to acutely increase brain workload/activity. They were able to dynamically measure increased glucose utilization with ^{18}F-FDG during intermittent visual stimuli as compared to resting conditions (12). Similarly, we were able to demonstrate increased ^{18}F-FDG uptake into the myocardium during hypoxia-induced increased myocardial workload. The only previous study to determine the effects of hypoxic stress on ^{18}F-FDG uptake in the heart during hypoxia used a bolus injection method and randomized human subjects into a normoxia or hypoxia group instead of scanning each subject under both conditions (24). Continuous infusion of ^{18}F-FDG enables a rest-stress scenario during a single dynamic imaging study.

One major advantage to our approach of continuous infusion is that we performed a rest-stress protocol in each animal with the use of ~5 mCi of radiotracer. Previous work that

Author Manuscript Author Manuscript Author Manuscript Author Manuscript

looked at rest and pharmacologic stress/cognitive task dependent changes in cerebral glucose metabolism used two separate PET scans which required a greater amount of radioactivity, in addition to increased intrasubject variability (14). Our study establishes the feasibility using continuous infusion of ^{18}F-FDG and PET/MR to determine cardiac glucose utilization and functional changes during normoxia rest and hypoxic stress in a single imaging session, which is a fundamental improvement over the standard bolus injection technique which may mitigate known intrasubject variability if rest and stress procedures are performed at different times rather than serially.

Furthermore, demonstrations of quantitative kinetic analysis using general linear model (GLM) approaches to Patlak using infused PET radiotracers have been previously reported (15), and these quantitative imaging outcomes as used herein, could be used to assess cardiac disease. In addition to using the quantitative kinetic approach with Patlak analysis, we also utilized a semi-quantitative approach to determining myocardial glucose uptake during rest and stress. The advantage of the semi-quantitative approach (slope ratio) used here is that it could be used in an environment that does not require the use of arterial sampling to estimate plasma ^{18}F-FDG activity. We found that the Ki values were of the same order of magnitude and of similar values as the slope ratio presented in this study, suggesting that this semi-quantitative approach may be a quick and practical means of determining metabolic changes in a clinical setting.

Until now, there have been very few studies using cardiac PET/MR and all of these studies have performed assessments of cardiac function and metabolism under resting conditions. However, in most cardiac conditions, cardiac dysfunction is best elicited with the use of stress, such as exercise (38–40). Therefore, we used the strength of PET/MR to develop a cardiac PET/MR stress test that may translate to studying human populations of cardiac disease. To our knowledge this was the first study to demonstrate significant changes in cardiac function and glucose utilization during a rest-stress scenario by combining dynamic imaging of cardiac function and glucose metabolism during a single scanning session. Future use of an MRI compatible exercise ergometers (41) during cardiac PET/MR scans may enable investigators and clinicians to unmask cardiometabolic and functional sequelae prior to clinical symptoms of disease or to assess prognosis of a disease state. Indeed, one study has used static PET acquisition to demonstrate increased ^{18}F-FDG uptake into the myocardium with exercise (42). One of the strengths of cardiac PET/MR is that it permits reconstruction of accurate fusion images to simultaneously study the tight coupling between metabolism and contractile function in the heart. Studies using a cardiac PET/MR stress test, similar to the approach herein, would permit investigators to obtain simultaneous measurements of cardiac (change in contractile function during stress) and metabolic reserve (change in substrate metabolism from rest to exercise) in order to more directly examine the relationship between cardiac contractile function and substrate metabolism. Previous work in a preclinical model of heart failure has demonstrated that increased reliance on glucose (i.e. glycolysis) was associated with reductions in contractile function at rest, yet at higher cardiac workloads the failing heart did not demonstrate further increases in glucose utilization as compared to control hearts suggesting a reduction in glucose metabolic reserve (33). These measures of cardiac substrate metabolism and contractile function during stress would permit a better understanding of the link between cardiac energetics and function in

Author Manuscript Author Manuscript Author Manuscript Author Manuscript

health and disease. For example, little is known about the progression of metabolic abnormalities throughout the stages of left or right heart failure and the use of a cardiac PET/MR stress test during early stages of heart failure would provide clinicians with a better understanding of pathological progression and may offer more prognostic value.

Limitations

This pilot study has demonstrated the feasibility of a rest-stress PET/MR imaging protocol to determine metabolic and functional changes in the myocardium, yet questions remain. For instance, this study was performed in anesthetized swine, and there is need to determine the feasibility of using a rest-stress scenario in human subjects. We assessed the slope of a time activity ratio function and the Patlak rate constant during the assumption of a metabolic steady state during rest and stress, which we acknowledge has potential limitations. For instance, as hypoxia exposure increased with time, we saw further increases in arterial lactate concentration which suggests further changes in whole body metabolism. This suggests that although, S_PO_2 was relatively constant after 10 minutes of hypoxia wash-in, cardiac glucose metabolism may not have been at steady state after extended hypoxia exposure. It is therefore possible that ^{18}F-FDG uptake by the heart was underestimated, especially in the final minutes of hypoxia exposure. Therefore, future work to measure dynamic changes of ^{18}F-FDG within the stress condition (e.g., early versus late stress) could address this potential limitation.

Another limitation is that we did not measure coronary flow/perfusion. Since we applied a stress it is likely that coronary perfusion changes occurred, especially when cardiac workload increased during hypoxia. A previous study determined the effect of enhanced coronary perfusion on ^{18}F-FDG uptake into the myocardium and found that increasing coronary flow with nitroprusside resulted in no changes in glucose uptake (43, 44). These results demonstrate that increasing flow without increasing myocardial workload does not result in an increase in metabolic fuel uptake. This is similar to a finding that used hypercapnia to stimulate cerebral blood flow and found that increased flow did not alter ^{18}F-FDG uptake rate into the brain (12). Given our application of steady state rest and stress conditions, we do not expect myocardial flow to change during each state, and thus it is unlikely that steady state changes in flow would change the slope of the time activity ratio functions. Additionally, arterial hypoxemia results in peripheral vasodilation and increased skeletal muscle blood flow (45, 46) which should further enhance ^{18}F-FDG uptake into the skeletal muscle, yet there was a decrease in the skeletal muscle to blood pool slope during hypoxia exposure. Taken together, these findings demonstrate that glucose uptake in striated muscle is regulated by metabolic demand when blood flow is not a limiting factor.

New Knowledge Gained

This study has demonstrated the feasibility of performing a cardiac PET/MR stress test which showed identifiable changes during simultaneous acquisition of cardiac metabolic and functional variables. This application has translational implications to the study of cardiac disease progression in human populations. Further development of this approach utilizing exercise as a physiological stressor in human subjects is warranted.

Author Manuscript Author Manuscript Author Manuscript Author Manuscript

Conclusion

In conclusion, this was the first study to our knowledge to develop a novel cardiac PET/MR stress test to determine dynamic changes by simultaneous measures of cardiac contractile function and glucose metabolism. Further work refining the kinetic modeling of the radiotracer and workflow for PET/MR during rest-stress scenarios is still needed, but the application for this novel non-invasive methodology has tremendous potential to elucidate mechanisms of human cardiac disease, in addition to the management of known disease states.

Acknowledgements

We would like to thank Dan Consigny, Sara John, Jenelle Fuller, and Kent MacLaughlin for their contributions to this study.

Research support was provided in part by University of Wisconsin-Madison School of Medicine and Public Health Department Research and Development Funds from the Departments of Pediatrics (Eldridge), Medicine (Goss) and Radiology (McMillan), as well as additional funding from the Wisconsin Alumni Research Foundation (Eldridge). Kara Goss and portions of the project are supported by the University of Wisconsin Clinical and Translational Science Award (CTSA) program, through the NIH National Center for Advancing Translational Sciences (NCATS), grant NIH UL1TR000427 (PI Dresher; 4KL2TR000428-10).

Abbreviations:

LV	left ventricle
RV	right ventricle
EF	ejection fraction
EDV	End-diastolic volume
ESV	End-systolic volume
^{18}F-FDG	^{18}F-fluorodexyglucose
TAC	time activity curve

References

(1). Bache RJ, Zhang J, Murakami Y, Zhang Y, Cho YK, Merkle H et al. Myocardial oxygenation at high workstates in hearts with left ventricular hypertrophy. Cardiovascular research 1999;42:616–26. [PubMed: 10533601]

(2). Chess DJ, Lei B, Hoit BD, Azimzadeh AM, Stanley WC. Effects of a high saturated fat diet on cardiac hypertrophy and dysfunction in response to pressure overload. Journal of cardiac failure 2008;14:82–8. [PubMed: 18226777]

(3). de las Fuentes L, Soto PF, Cupps BP, Pasque MK, Herrero P, Gropler RJ et al. Hypertensive left ventricular hypertrophy is associated with abnormal myocardial fatty acid metabolism and myocardial efficiency. Journal of nuclear cardiology : official publication of the American Society of Nuclear Cardiology 2006;13:369–77. [PubMed: 16750782]

(4). Doenst T, Pytel G, Schrepper A, Amorim P, Färber G, Shingu Y et al. Decreased rates of substrate oxidation ex vivo predict the onset of heart failure and contractile dysfunction in rats with pressure overload. Cardiovascular research 2010;86:461–70. [PubMed: 20035032]

Author Manuscript Author Manuscript Author Manuscript Author Manuscript

(5). Fu Y-n, Xiao H, Ma X-w, Jiang S-y, Xu M, Zhang Y-y. Metformin attenuates pressure overload-induced cardiac hypertrophy via AMPK activation. Acta pharmacologica Sinica 2011;32:879–87. [PubMed: 21552292]

(6). Kundu BK, Zhong M, Sen S, Davogustto G, Keller SR, Taegtmeyer H. Remodeling of glucose metabolism precedes pressure overload-induced left ventricular hypertrophy: review of a hypothesis. Cardiology 2015;130:211–20. [PubMed: 25791172]

(7). Sen S, Kundu BK, Wu HC-J, Hashmi SS, Guthrie P, Locke LW et al. Glucose regulation of load-induced mTOR signaling and ER stress in mammalian heart. Journal of the American Heart Association 2013;2:e004796. [PubMed: 23686371]

(8). Zhabyeyev P, Gandhi M, Mori J, Basu R, Kassiri Z, Clanachan A et al. Pressure-overload-induced heart failure induces a selective reduction in glucose oxidation at physiological afterload. Cardiovascular research 2013;97:676–85. [PubMed: 23257023]

(9). Zhong M, Alonso CE, Taegtmeyer H, Kundu BK. Quantitative PET Imaging Detects Early Metabolic Remodeling in a Mouse Model of Pressure-Overload Left Ventricular Hypertrophy In Vivo. Journal of Nuclear Medicine 2013;54:609–15. [PubMed: 23426760]

(10). Yang T, Wang L, Xiong C-M, He J-G, Zhang Y, Gu Q et al. The ratio of (18)F-FDG activity uptake between the right and left ventricle in patients with pulmonary hypertension correlates with the right ventricular function. Clinical nuclear medicine 2014;39:426–30. [PubMed: 24662662]

(11). Taylor M, Wallhaus TR, Degrado TR, Russell DC, Stanko P, Nickles RJ et al. An evaluation of myocardial fatty acid and glucose uptake using PET with [18F]fluoro-6-thia-heptadecanoic acid and [18F]FDG in Patients with Congestive Heart Failure. Journal of nuclear medicine : official publication, Society of Nuclear Medicine 2001;42:55–62.

(12). Villien M, Wey H-Y, Mandeville JB, Catana C, Polimeni JR, Sander CY et al. Dynamic functional imaging of brain glucose utilization using fPET-FDG. NeuroImage 2014;100:192–9. [PubMed: 24936683]

(13). Brooks RA, Di Chiro G, Zukerberg BW, Bairamian D, Larson SM. Test-retest studies of cerebral glucose metabolism using fluorine-18 deoxyglucose: validation of method. J Nucl Med 1987;28:53–9. [PubMed: 3491886]

(14). Schmidt ME, Ernst M, Matochik JA, Maisog JM, Pan BS, Zametkin AJ et al. Cerebral glucose metabolism during pharmacologic studies: test-retest under placebo conditions. J Nucl Med 1996;37:1142–9. [PubMed: 8965185]

(15). Hahn A, Gryglewski G, Nics L, Hienert M, Rischka L, Vraka C et al. Quantification of task-specific glucose metabolism with constant infusion of 18F-FDG. J Nucl Med 2016.

(16). Boos CJ, Mellor A, O'Hara JP, Tsakirides C, Woods DR. The Effects of Sex on Cardiopulmonary Responses to Acute Normobaric Hypoxia. High Alt Med Biol 2016;17:108–15. [PubMed: 27008376]

(17). Fleg JL, O'Connor F, Gerstenblith G, Becker LC, Clulow J, Schulman SP et al. Impact of age on the cardiovascular response to dynamic upright exercise in healthy men and women. Journal of applied physiology (Bethesda, Md : 1985) 1995;78:890–900.

(18). Patlak CS, Blasberg RG, Fenstermacher JD. Graphical evaluation of blood-to-brain transfer constants from multiple-time uptake data. J Cereb Blood Flow Metab 1983;3:1–7. [PubMed: 6822610]

(19). Bøtker HE, Böttcher M, Schmitz O, Gee A, Hansen SB, Cold GE et al. Glucose uptake and lumped constant variability in normal human hearts determined with [18F]fluorodeoxyglucose. J Nucl Cardiol 1997;4:125–32. [PubMed: 9115064]

(20). Dedobbeleer C, Hadefi A, Naeije R, Unger P. Left ventricular adaptation to acute hypoxia: a speckle-tracking echocardiography study. Journal of the American Society of Echocardiography : official publication of the American Society of Echocardiography 2013;26:736–45. [PubMed: 23706341]

(21). Allemann Y, Rotter M, Hutter D, Lipp E, Sartori C, Scherrer U et al. Impact of acute hypoxic pulmonary hypertension on LV diastolic function in healthy mountaineers at high altitude. Am J Physiol Heart Circ Physiol 2004;286:H856–62. [PubMed: 14604853]

Author Manuscript Author Manuscript Author Manuscript Author Manuscript

(22). Boos CJ, Hodkinson PD, Mellor A, Green NP, Bradley D, Greaves K et al. The effects of prolonged acute hypobaric hypoxia on novel measures of biventricular performance. Echocardiography (Mount Kisco, NY) 2013;30:534–41.

(23). Goebel B, Handrick V, Lauten A, Fritzenwanger M, Schutze J, Otto S et al. Impact of acute normobaric hypoxia on regional and global myocardial function: a speckle tracking echocardiography study. Int J Cardiovasc Imaging 2013;29:561–70. [PubMed: 22918573]

(24). Chen CH, Liu YF, Lee SD, Huang CY, Lee WC, Tsai YL et al. Altitude hypoxia increases glucose uptake in human heart. High Alt Med Biol 2009;10:83–6. [PubMed: 19278356]

(25). Axel L, Dougherty L. MR imaging of motion with spatial modulation of magnetization. Radiology 1989;171:841–5. [PubMed: 2717762]

(26). Clark NR, Reichek N, Bergey P, Hoffman EA, Brownson D, Palmon L et al. Circumferential myocardial shortening in the normal human left ventricle. Assessment by magnetic resonance imaging using spatial modulation of magnetization. Circulation 1991;84:67–74. [PubMed: 2060124]

(27). Young AA, Imai H, Chang CN, Axel L. Two-dimensional left ventricular deformation during systole using magnetic resonance imaging with spatial modulation of magnetization. Circulation 1994;89:740–52. [PubMed: 8313563]

(28). Sengupta PP, Krishnamoorthy VK, Korinek J, Narula J, Vannan MA, Lester SJ et al. Left ventricular form and function revisited: applied translational science to cardiovascular ultrasound imaging. Journal of the American Society of Echocardiography : official publication of the American Society of Echocardiography 2007;20:539–51. [PubMed: 17485001]

(29). Carreras F, Ballester M, Pujadas S, Leta R, Pons-Llado G. Morphological and functional evidences of the helical heart from non-invasive cardiac imaging. European journal of cardio-thoracic surgery : official journal of the European Association for Cardio-thoracic Surgery 2006;29 Suppl 1:S50–5. [PubMed: 16563788]

(30). Poveda F, Gil D, Marti E, Andaluz A, Ballester M, Carreras F. Helical structure of the cardiac ventricular anatomy assessed by diffusion tensor magnetic resonance imaging with multiresolution tractography. Revista espanola de cardiologia (English ed) 2013;66:782–90. [PubMed: 24773858]

(31). Gao C, Lu K, Ye W, Li L, Cheng L. Reconstruction of the architecture of ventricular myocardial fibers in ex vivo human hearts. The heart surgery forum 2009;12:E225–9. [PubMed: 19683994]

(32). Carreras F, Garcia-Barnes J, Gil D, Pujadas S, Li CH, Suarez-Arias R et al. Left ventricular torsion and longitudinal shortening: two fundamental components of myocardial mechanics assessed by tagged cine-MRI in normal subjects. Int J Cardiovasc Imaging 2012;28:273–84. [PubMed: 21305357]

(33). Allard MF, Schonekess BO, Henning SL, English DR, Lopaschuk GD. Contribution of oxidative metabolism and glycolysis to ATP production in hypertrophied hearts. Am J Physiol 1994;267:H742–50. [PubMed: 8067430]

(34). Goodwin GW, Taylor CS, Taegtmeyer H. Regulation of energy metabolism of the heart during acute increase in heart work. J Biol Chem 1998;273:29530–9. [PubMed: 9792661]

(35). Wheeler TJ. Translocation of glucose transporters in response to anoxia in heart. J Biol Chem 1988;263:19447–54. [PubMed: 3058699]

(36). Lopaschuk G Regulation of carbohydrate metabolism in ischemia and reperfusion. Am Heart J 2000;139:S115–9. [PubMed: 10650324]

(37). Lopaschuk GD, Ussher JR, Folmes CDL, Jaswal JS, Stanley WC. Myocardial fatty acid metabolism in health and disease. Physiological reviews 2010;90:207–58. [PubMed: 20086077]

(38). Guazzi M, Myers J, Peberdy MA, Bensimhon D, Chase P, Arena R. Cardiopulmonary exercise testing variables reflect the degree of diastolic dysfunction in patients with heart failure-normal ejection fraction. Journal of cardiopulmonary rehabilitation and prevention 2010;30:165–72. [PubMed: 20216325]

(39). Kitzman DW, Higginbotham MB, Cobb FR, Sheikh KH, Sullivan MJ. Exercise intolerance in patients with heart failure and preserved left ventricular systolic function: failure of the Frank-Starling mechanism. Journal of the American College of Cardiology 1991;17:1065–72. [PubMed: 2007704]

Author Manuscript Author Manuscript Author Manuscript Author Manuscript

(40). Nedeljkovic I, Banovic M, Stepanovic J, Giga V, Djordjevic-Dikic A, Trifunovic D et al. The combined exercise stress echocardiography and cardiopulmonary exercise test for identification of masked heart failure with preserved ejection fraction in patients with hypertension. European journal of preventive cardiology 2015:1–11.

(41). Forouzan O, Warczytowa J, Wieben O, Francois CJ, Chesler NC. Non-invasive measurement using cardiovascular magnetic resonance of changes in pulmonary artery stiffness with exercise. J Cardiovasc Magn Reson 2015;17:109. [PubMed: 26653289]

(42). Kemppainen J, Fujimoto T, Kalliokoski KK, Viljanen T, Nuutila P, Knuuti J. Myocardial and skeletal muscle glucose uptake during exercise in humans. J Physiol 2002;542:403–12. [PubMed: 12122141]

(43). Law WR, Raymond RM. Adenosine potentiates insulin-stimulated myocardial glucose uptake in vivo. Am J Physiol 1988;254:H970–5. [PubMed: 3284395]

(44). Mainwaring R, Lasley R, Rubio R, Wyatt DA, Mentzer RM, Jr. Adenosine stimulates glucose uptake in the isolated rat heart. Surgery 1988;103:445–9. [PubMed: 3281300]

(45). Richards JC, Crecelius AR, Larson DG, Luckasen GJ, Dinenno FA. Impaired peripheral vasodilation during graded systemic hypoxia in healthy older adults: role of the sympathoadrenal system. Am J Physiol Heart Circ Physiol 2017;312:H832–h41. [PubMed: 28159810]

(46). Weisbrod CJ, Minson CT, Joyner MJ, Halliwill JR. Effects of regional phentolamine on hypoxic vasodilatation in healthy humans. J Physiol 2001;537:613–21. [PubMed: 11731591]

Author Manuscript Author Manuscript Author Manuscript Author Manuscript

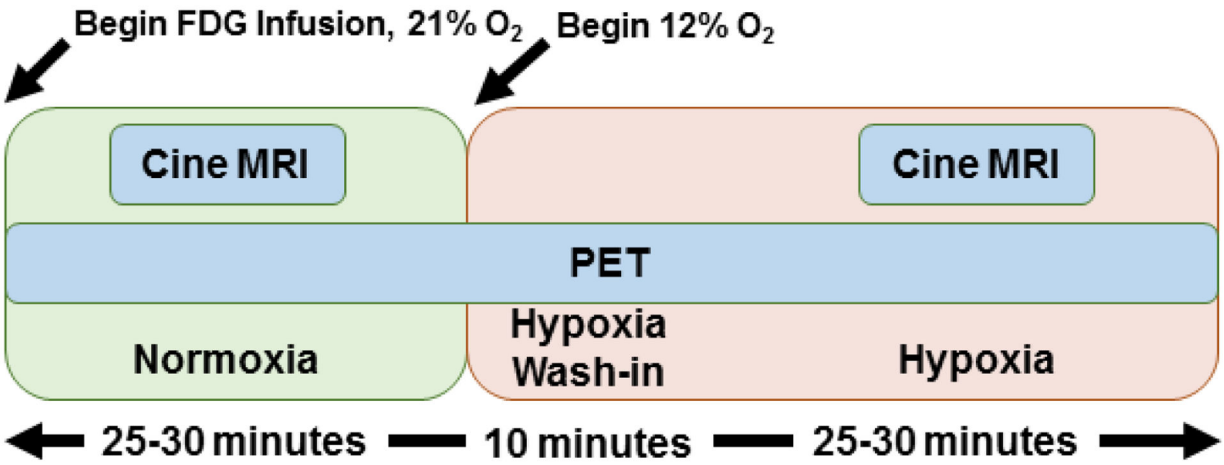

Figure 1:
Study schema demonstrating the administration of hypoxic stress with dynamic PET/MR imaging.

Author Manuscript Author Manuscript Author Manuscript Author Manuscript

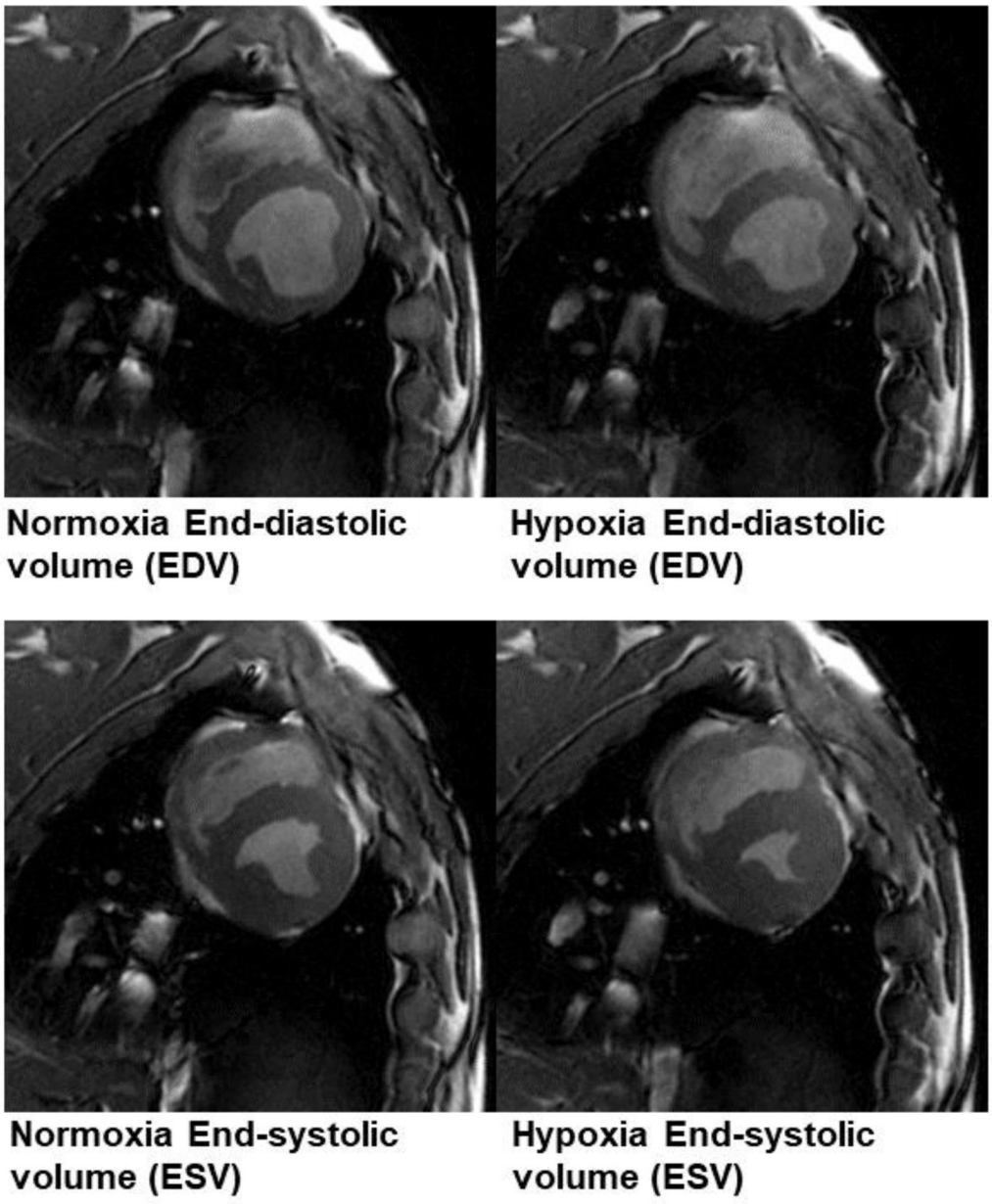

Figure 2:
Example cine MR imaging at end diastole (top) and end systole (bottom). During hypoxia, there was a decline in both the end-diastolic volume (EDV) and end-systolic volume (ESV). ESV declined to a greater extent than did EDV.

Author Manuscript Author Manuscript Author Manuscript Author Manuscript

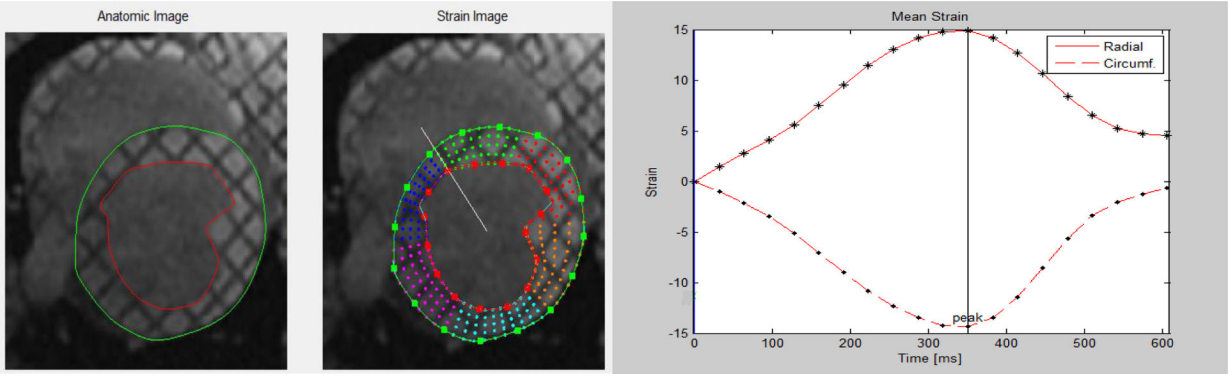

Figure 3:

Representative image of LV strain analysis from tagged short-axis cine images (left) and circumferential and radial strain curves (right).

Author Manuscript Author Manuscript Author Manuscript Author Manuscript

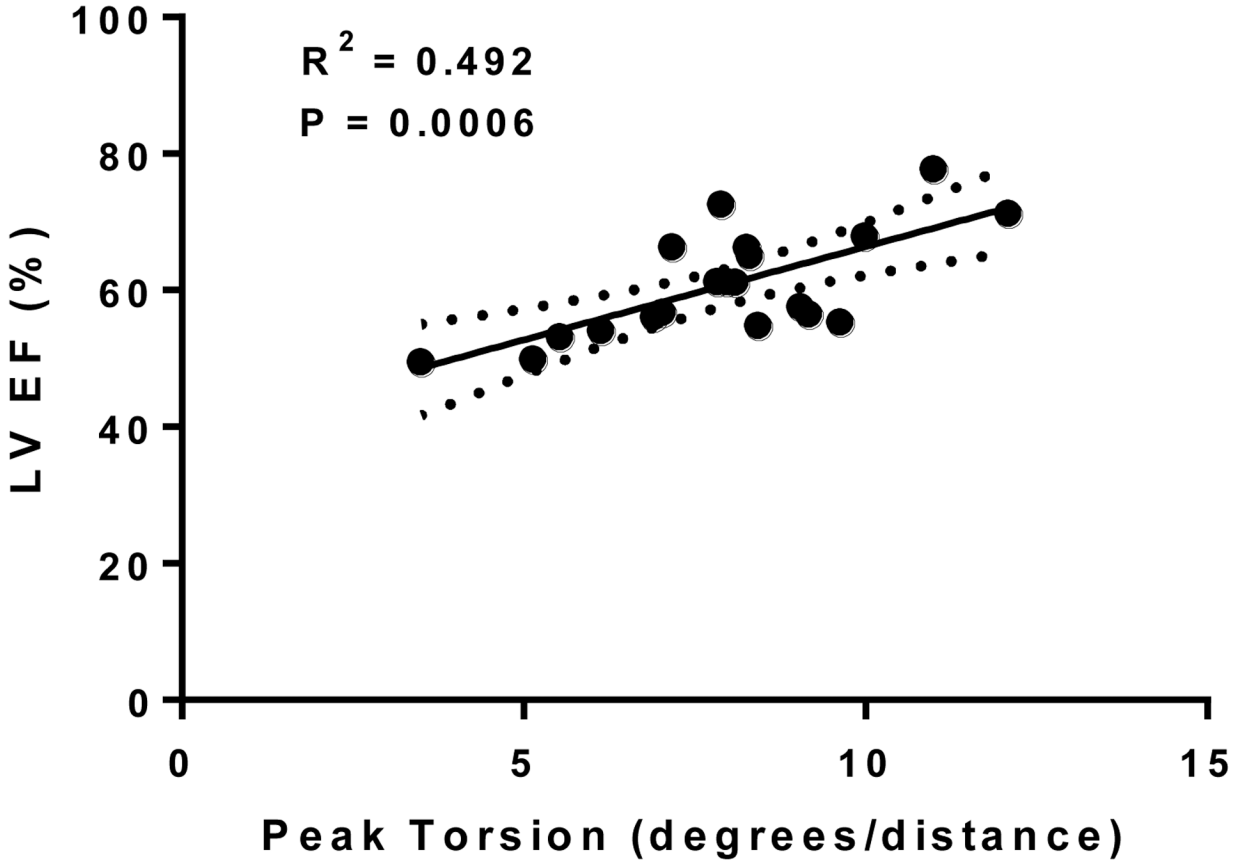

Figure 4:
Relationship between LV EF and peak torsion.

Author Manuscript Author Manuscript Author Manuscript Author Manuscript

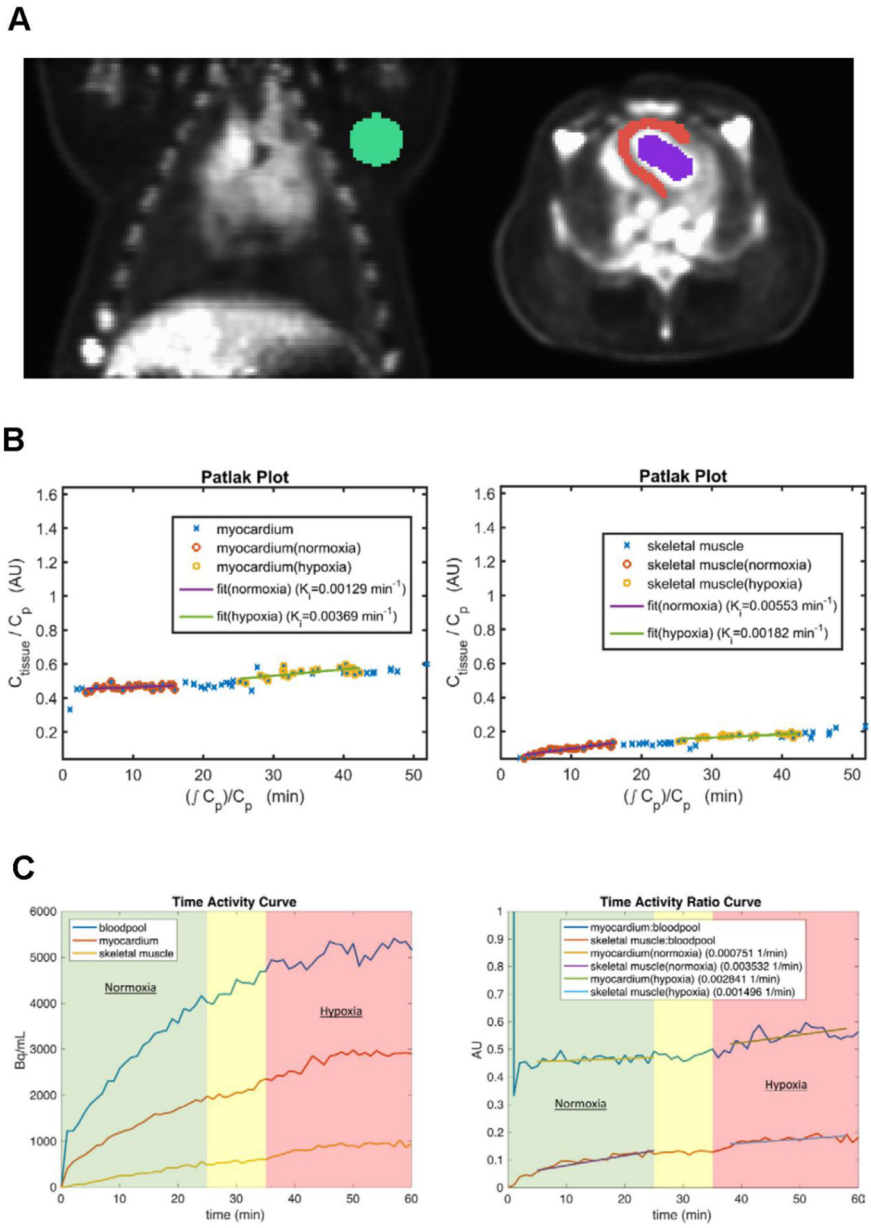

Figure 5:

(A) Representative images of the ROIs drawn for the skeletal muscle (green), myocardium (red) and bloodpool (blue). **(B)** Patlak plots for the myocardium (left) and skeletal muscle (right) during the rest-stress protocol. These plots show an increase in the Ki (myocardium) and a decrease in the Ki (skeletal muscle) during hypoxia. **(C)** Example time activity curve during ^{18}F-FDG infusion showing time activity in the left ventricular bloodpool, left ventricle (myocardium), and skeletal muscle (left). Example time activity ratio curve (obtained by normalization to the bloodpool time activity curve) for myocardium and skeletal muscle (right). The slope of the myocardium time activity ratio during hypoxia is increased relative to normoxia and to skeletal muscle. The green background reflects time in normoxic breathing, the red background reflects time in hypoxic breathing, and the yellow

Author Manuscript Author Manuscript Author Manuscript Author Manuscript

background reflects time spent waiting for the hypoxic steady state (i.e., hypoxic gas administration began at 25 minutes).

Author Manuscript Author Manuscript Author Manuscript Author Manuscript

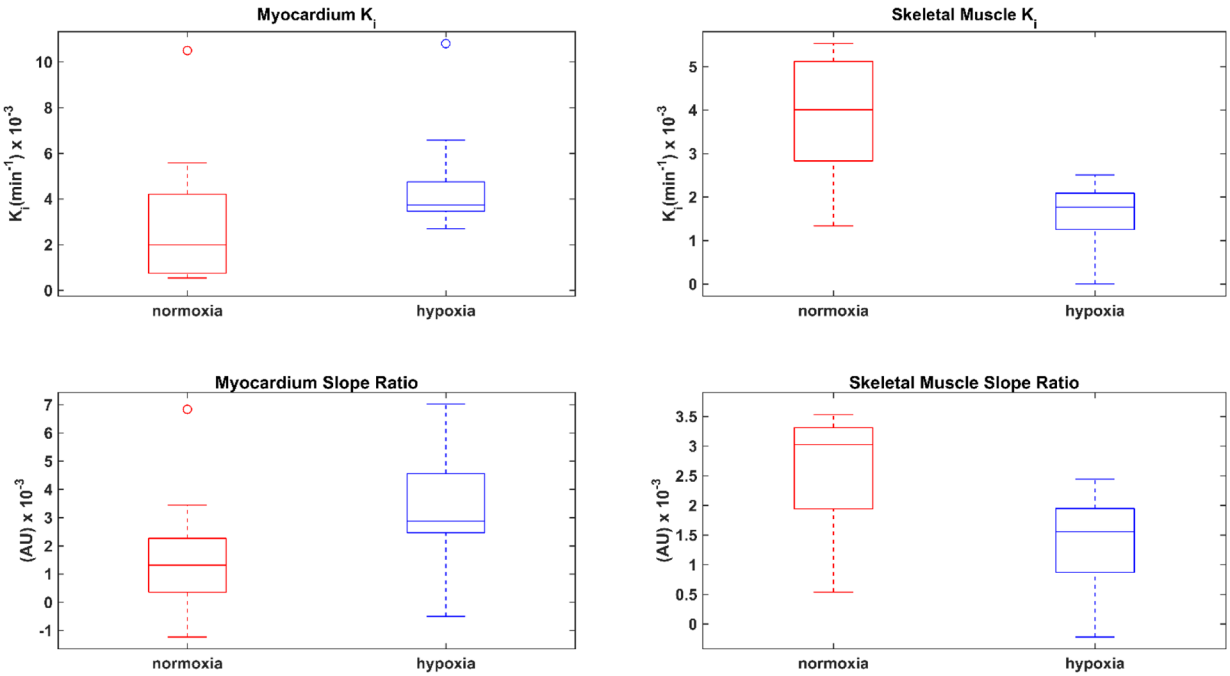

Figure 6:

Box plots represent the median (central mark) and the edges of the box are the 25th and 75th percentiles, the whiskers extend to the most extreme data points not considered outliers, and outliers (open circles) are plotted individually in normoxia (red) and hypoxia (blue). Patlak rate constant (Ki) (top row) show a significant hypoxic-dependent increase in the myocardial uptake rate and a decrease in the skeletal muscle uptake rate. Box plots show changes that are similar in magnitude and direction as determined by the Patlak rate constant (Ki) during hypoxia in the myocardium:blood pool and skeletal muscle: blood pool slope ratios (bottom row). Refer to Table III for relevant p-values for Ki and slope ratio.

Author Manuscript Author Manuscript Author Manuscript Author Manuscript

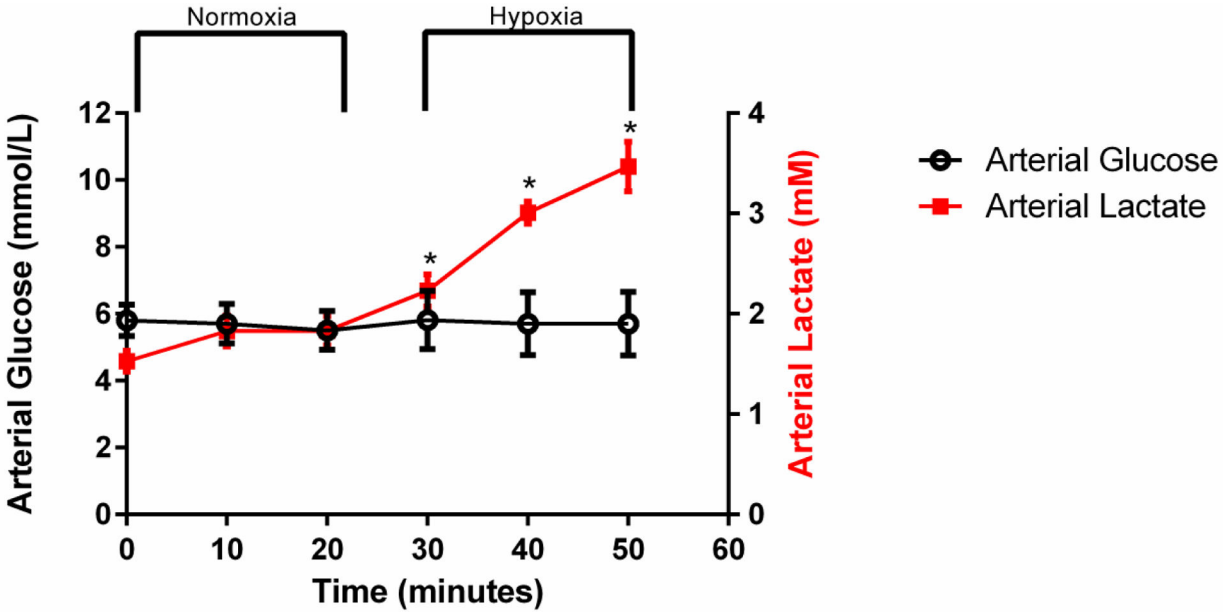

Figure 7:

Plasma obtained from the carotid artery was used to determine changes in glucose and lactate during the rest-stress protocol. There were no differences in arterial plasma glucose over time, while hypoxia induced an increase in arterial plasma lactate. Values represent Mean ± SEM. * indicates significant increases in arterial plasma lactate during hypoxic stress compared to resting conditions ($p < 0.05$)

Author Manuscript

Author Manuscript

Author Manuscript

Author Manuscript

Table I:

Cardiovascular hemodynamic changes from normoxia to hypoxia (n = 10). Values represent Mean ± SEM.

	Normoxia	Hypoxia	% Change	p-value
Heart Rate (beats/min)	97 ± 3	112 ± 4	14.7 ± 2.9	0.0005
Cardiac Output (ml/min)	3228 ± 145	3931 ± 288	21.0 ± 5.9	0.0060
LV EDV (ml)	61 ± 3	54 ± 3	−11.1 ± 3.1	0.0027
LV ESV (ml)	27 ± 2	18 ± 2	−30.2 ± 6.9	0.0006
LV SV (ml)	33 ± 1	35 ± 2	5.7 ± 3.3	0.1065
LV EF (%)	56 ± 1	66 ± 2	19.0 ± 4.2	0.0016
SBP (mmHg)	113 ± 5	111 ± 6	−1.3 ± 2.7	0.6400
DBP (mmHg)	41 ± 2	40 ± 2	−3.2 ± 5.2	0.4690
MAP (mmHg)	65 ± 3	63 ± 3	−2.9 ± 3.6	0.4138
Rate Pressure Product (mmHg*bpm)	10767 ± 740	12759 ± 1138	18.3 ± 6.3	0.0233
SpO_2	99 ± 0.2	71 ± 1.7	−27.8 ± 1.7	0.0001

Author Manuscript

Author Manuscript

Author Manuscript

Author Manuscript

Table II:

Left ventricular strain parameters in normoxia and hypoxia (n = 10). Values represent Mean ± SEM.

	Normoxia (21% O_2)	Hypoxia (12% O_2)	% Change	p-value
Mean peak circumferential strain (%)	−12.66 ± 0.43	−12.82 ± 0.32	1.77 ± 2.43	0.8457
Circumferential systolic strain rate (%/s)	−62.74 ± 2.27	−59.26 ± 2.13	−4.92 ± 3.53	0.2324
Circumferential diastolic strain rate (%/s)	82.91 ± 3.13	78.61 ± 4.78	−5.50 ± 3.71	0.2754
Mean peak radial strain (%)	10.73 ± 0.81	11.60 ± 0.71	12.43 ± 9.66	0.2754
Radial systolic strain rate (%/s)	52.80 ± 3.36	55.76 ± 4.21	10.17 ± 11.54	0.5566
Radial diastolic strain rate (%/s)	−52.44 ± 3.56	−45.60 ± 5.51	−8.31 ± 14.04	0.4316
Peak rotation (degrees)	4.62 ± 0.44	6.06 ± 0.41	42.34 ± 19.24	0.0059
Peak torsion (degrees/distance)	7.10 ± 0.60	8.79 ± 0.57	34.06 ± 18.13	0.0371

Author Manuscript

Author Manuscript

Author Manuscript

Author Manuscript

Table III.

Myocardial and skeletal muscle glucose utilization rate as measured by the two-compartment Patlak model. Slope of time activity curves in the myocardium and skeletal muscle normalized to the blood pool slope in normoxia and hypoxia (n = 10). Values represent Mean ± SEM.

	Normoxia (21% O_2)	Hypoxia (12% O_2)	% Change	p-value
Myocardial K_i	0.0031 ± 0.0010	0.0047 ± 0.0008	167 ± 58	0.0098
Skeletal Muscle K_i	0.0038 ± 0.0004	0.0016 ± 0.0002	−47 ± 16	0.0059
Blood pool (Bq/cc/min)	96.89 ± 15.22	21.18 ± 7.57	−78 ± 13	0.0098
Myocardium:Blood pool	0.0017 ± 0.0007	0.0033 ± 0.0007	261 ± 124	0.0020
Skeletal Muscle:Blood pool	0.0026 ± 0.0003	0.0014 ± 0.0002	−23 ± 27	0.0195